

Article

# Cutting Speed and Feed Influence on Surface Microhardness of Dry-Turned UNS A97075-T6 Alloy

Sergio Martín-Béjar , Francisco Javier Trujillo Vilches \* , Carolina Bermudo Gamboa   
and Lorenzo Sevilla Hurtado 

Department of Civil, Material and Manufacturing Engineering, EII, University of Malaga, C/Dr. Ortiz Ramos s/n, E-29071 Malaga, Spain; smartinb@uma.es (S.M.-B.); bgamboa@uma.es (C.B.G.); lsevilla@uma.es (L.S.H.)

\* Correspondence: trujillov@uma.es; Tel.: +34-951-952-245

Received: 23 December 2019; Accepted: 23 January 2020; Published: 5 February 2020



**Abstract:** In this work, an analysis of the cutting speed and feed influence on surface roughness and microhardness of UNS A97075-T6 alloy, turned under dry conditions, was carried out. The results were compared before and after a corrosion process. The influence of these cutting parameters on each of these variables was analyzed, as well as the possible interrelation between them. The microgeometrical deviations showed a general trend to increase with feed. However, no significant modifications were observed as a function of the cutting speed. This trend was softer after the corrosion process, due to the surface alterations produced by pitting corrosion, which resulted in higher dispersion of the experimental data. In addition, a surface microhardness increment was observed in all samples, after machining and before corrosion, regardless of the cutting parameter values. The experimental results revealed that the mechanical effects, produced by the feed, should not be neglected against the thermal effects, produced by the cutting speed, within the range of the tested cutting speed. Finally, the corrosion process negatively affected the microhardness, but it was not possible to establish a direct relationship between the cutting parameters, surface roughness, and microhardness after a corrosion process.

**Keywords:** dry turning; surface roughness; microhardness; UNS A97075; aluminum alloys

## 1. Introduction

Pure aluminum or aluminum with a very low weight percentage of alloying elements (1000 series) has, among its mechanical properties, a low wear resistance and a low hardness. Therefore, the addition of alloying elements implies an improvement of the aluminum surface characteristics and mechanical properties, making these alloys one of the most used materials in the industrial activity [1]. One of the industrial sectors in which aluminum alloys are of great interest is the aeronautical industry. Their excellent density and mechanical properties make this type of material suitable for the manufacturing of aircraft structural elements. In particular, the 2000 (Al–Cu) and 7000 (Al–Zn) series are widely used for structural elements in the wings, the fuselage, or the tail of the aircraft [2]. These structural components are usually high-rigidity elements and, frequently, they need to be manufactured in one piece. In these cases, the machining operations are usually quite competitive from a productive point of view. In particular, milling operations are used for large pocketing operations in rib-shaped elements, drilling operations are frequent in the machining of holes for rivets, and turning operations are used to manufacture coupled parts with cylindrical shapes [3].

Machining operations result in alterations in the surface of the stock material. These alterations not only affect their geometrical characteristics (at macro and micro scale) but also modify the physical–chemical and mechanical properties of the surface (residual stresses, microstructural alterations, cracks and microcracks, microhardness, corrosion resistance, etc.) [4–6]. All these alterations (both material properties and geometry) are part of the surface integrity concept [7–9], which is one

of the most valued aspects from the point of view of quality requirements, especially in structural elements for aircraft, where these requirements are very high due to functionality and reliability reasons [10].

Lubricants or coolants, applied during the machining process (cutting fluids), are traditionally used to increase the productivity of these processes and the machined part functionality. However, the current trend regarding the use of sustainable manufacturing technologies led to a reduction in the use of these highly polluting substances. This resulted in the application of more efficient techniques, such as MQL (minimum quantity lubricant), or the total suppression of these substances (dry machining) [11–15]. In addition, aluminum alloys are frequently used hybridized with other materials, such as carbon fiber-reinforced polymers (CFRP) or titanium, to form structural elements, such as fiber metal laminates (FML) [16]. In those cases, the chip recycling (mixture of metal, carbon fiber, and cutting fluids) becomes complex and expensive. In addition, it should be pointed that CFRPs do not exhibit good behavior under the cutting fluid action [17].

However, in dry machining, the thermal effects become more relevant compared to the effects of plastic deformation due to mechanical actions on the surface. This results in greater surface alterations at both microstructural and geometric levels [18–20]. Due to the high importance of the surface state in phenomena such as crack and microcrack initiation, which can affect significant properties such as fatigue resistance or corrosion [21], it is necessary to analyze the effect of the machining input variables on the machined part surface integrity.

Thus, the surface microhardness of aircraft structural components is particularly relevant, given their influence on the bearing capacity and the wear resistance of these elements [22,23]. In this sense, the cutting parameters are some of the most important machining input variables to keep in mind regarding this output variable. Although there are numerous works in the literature that analyzed the influence of cutting parameters on surface microhardness [24–26], these studies should be completed in the case of dry machining of aluminum alloys.

Thus, Kurkute et al. [27] analyzed the feed and cutting speed influence on the cutting forces and the surface roughness of the UNS A96063 alloy, in dry-turning operations, in order to obtain the optimal machining conditions for low surface roughness ( $R_a$ ) and high surface microhardness ( $HV$ ). Cutting speed values between 10 and 50 m/min and feed values between 0.40 and 0.80 mm/r were used. A lower roughness and higher microhardness were obtained for intermediate feed (0.5 mm/r) and high cutting speed values (40 m/min). In addition, a potential model was developed in this work. That model allowed obtaining the microhardness as a function of the feed rate, the cutting speed, the cutting forces, and the number of machining steps (roughing and finishing).

Surya et al. [28] analyzed the cutting speed and cutting depth influence on the microhardness of dry-turned UNS A97075 alloy. Different cutting speed (50, 100, 200 and 300 m/min) and cutting depth values (0.3, 0.6 and 0.9 mm) were used, whereas the feed remained constant (0.05 mm/r). In this case, a surface microhardness decrease was observed when the cutting speed was increased. In addition, a reduction in the microhardness was also observed when the cutting depth was increased, but its influence was less noticeable. The authors attributed this behavior to the heat generation and dissipation on the machined surface.

As previously mentioned, the machining operation modifies the surface microstructure of the machined parts. In this regard, Rotella et al. [29] used microhardness measurements to evaluate the depth reached by these microstructural alterations, in the dry turning of UNS A97075-T651 alloy. Several hardness tests were carried out for different surface layer depths (up to 500  $\mu\text{m}$ ). A microhardness reduction was observed as a function of the depth, and it was finally stabilized at greater depths. The cutting speed and the tool-tip radius influence was also analyzed. The results obtained showed that higher cutting speed values resulted in greater microstructure modifications, with a reduction in the grain size. In addition, cutting tools with higher tool-tip radius generated a greater reduction in the grain size and higher values of surface microhardness, as a consequence of the contact surface reduction between the tool and the machined part.

Similarly, Campbell et al. studied the microstructure modifications as a function of the surface microhardness, in the dry turning of UNS A97075-T651 alloy [30]. In this case, the turning operations were carried out with a constant feed (0.076 mm/r) and cutting speed values between 360 and 720 m/min, while also varying the tool rake angle ( $0^{\circ}$ – $15^{\circ}$ ). The authors indicated that the cutting speed increments and low tool rake angle generated a microstructure modification at higher surface depths, as a consequence of the temperature increment in the cutting area. Contrary to the results obtained by Rotella et al. in [29], Campbell [30] stated that the microhardness in a closer area to the surface decreased until 50- $\mu$ m depth. Once this value was reached, the microhardness tended to stabilize at higher values than the initial ones and, therefore, a more homogeneous microstructure was obtained.

With regard to the UNS A96061 alloy, Akkurt et al. [26] performed different conventional and non-conventional machining tests, in order to study the microhardness alterations induced by the process in the part surface. It was observed that, in all tested machining processes, the microhardness decreased in the most superficial layer of the machined part, compared to the starting material. This microhardness reduction is justified by the thermal effect of the machining operation on the machined surface. Moreover, this thermal effect is more important in surfaces that present greater irregularities and, therefore, less superficial microhardness.

On the other hand, 7000 aluminum alloy series have lower corrosion resistance compared to pure aluminum. Its main alloying element is Zn (~6%), which makes the appearance of the alumina protective layer (with higher corrosion resistance) more difficult [31]. For the 2000 and 7000 series, corrosion is usually localized, with the appearance of pitting common, as well as intergranular corrosion, which can be considered as the generation and nucleation points of microcracks that affect the continuity of the surface microstructure [32–34].

Despite the lack of research studying the cutting parameter influence on corrosion behavior of machined parts, several studies revealed that low cutting speed and high feed values result in machined parts with lower corrosion resistance [35–37]. In addition, the surface microhardness has a close connection with corrosion resistance. The metallic material corrosion resistance depends essentially on the ability to form passive bonded layers and its mechanical properties. Usually, higher hardness and tensile strength can be related to higher corrosion resistance [36,38,39].

Yue et al. [40] studied the effect of the immersion corrosion process (saline solution 3.5% NaCl) in parts of the UNS A92009 alloy, machined using three different techniques: turned with ceramic tool, turned with diamond tip tool, and WEDM (wire electrical discharge machining). The results revealed that the samples machined by WEDM showed less corrosion resistance than the turned ones. The authors justified this result due to the greater surface irregularity obtained after WEDM machining. In addition, turned parts with the diamond tool were less affected by the corrosion process.

Welcome et al. [41] evaluated the cutting parameters influence on the corrosion behavior of the UNS A92024-T3 aluminum alloy. After machining, the specimens were submerged in a saline solution (3.5% NaCl). Then, the surface finish after corrosion was compared with the initial one (after machining). The results showed that the use of lower feed and higher cutting speed resulted in a better corrosion resistance, as a consequence of the better surface quality of the machined parts.

As shown in the literature review, there are several studies that related the cutting parameters to surface properties such as microhardness and corrosion resistance in dry-machined aeronautical aluminum alloys. However, few studies included the feed as a parameter of influence. This may be logical, keeping in mind that most of these studies were carried out at high cutting speed values (above 100 m/min), where thermal effects (mainly influenced by the cutting speed) predominate over mechanical effects, in which the feed has a greater influence. However, as previously mentioned, these alloys are frequently used hybridized with other materials, such as CFRP and Ti, which require the application of lower cutting speeds. In addition, in no case were the synergistic effects between cutting parameters, geometric alterations, microhardness, and corrosion resistance analyzed.

Therefore, an analysis of cutting speed and feed influence on surface roughness and microhardness of UNS A97075-T6 alloy, turned under dry conditions, was carried out in this work. The results were

compared before and after a corrosion process. The influence of these cutting parameters on each of these variables (surface roughness, microhardness, and corrosion resistance) was analyzed, as well as the possible interrelation between them.

## 2. Materials and Methods

Several dry-turning tests were carried out in order to evaluate the cutting parameter influence on the surface microhardness of the aluminum alloy UNS A97075-T6. The tested alloy composition (% mass), obtained by arc atomic emission spectroscopy (AES), is shown in Table 1.

**Table 1.** Evaluated aluminum–zinc alloy UNS A97075-T6 composition (% weight).

Zn	Mg	Cu	Cr	Si	Mn	Al
6.03	2.62	1.87	0.19	0.09	0.07	Balance

Cylindrical bars (diameter,  $D = 20$  mm; length,  $L = 110$  mm) were used as stock geometry to manufacture the specimens. The sample final geometry is shown in Figure 1a. A step (25-mm length) was machined at the end of the specimen, in order to ensure a proper grip to the chuck (Figure 1b). A length of 65 mm was turned as the microhardness measurement area. The starting diameter was reduced to 17 mm in two stages. Firstly, a roughing operation was performed to reach 18 mm; then, a finishing operation was carried out to reduce the diameter to 17 mm. A new tool was used in this last operation, to ensure the same initial conditions. The machining operations were carried out in a CNC turning center.

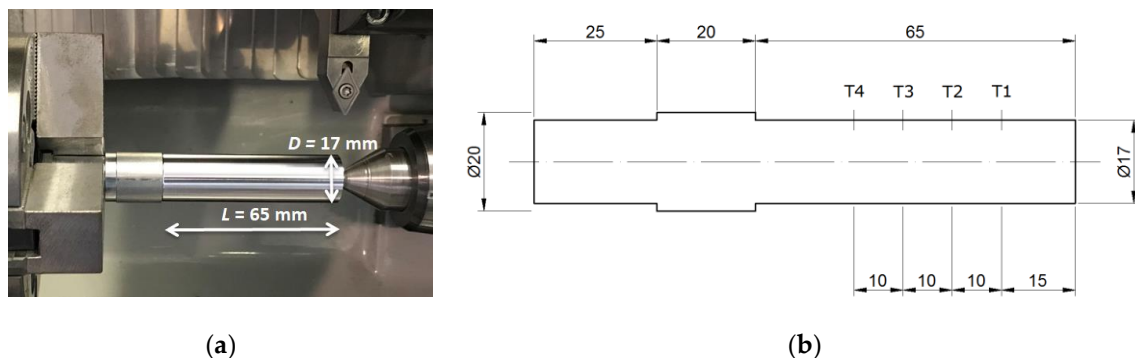


**Figure 1.** (a) Sample geometry; (b) measurement area (all dimensions in mm).

Different cutting parameter values were used to perform the finishing step. Their values are shown in Table 2. The cutting depth ( $a_p$ ) remained constant in every test. To evaluate the thermo-mechanical effects of the cutting parameters on the surface micro-hardness, several values of cutting speed ( $v_c$ ) and feed ( $f$ ) were used. As previously commented, it is necessary to emphasize that, although this alloy is not usually machined with low cutting speed values, its use hybridized with other materials forces the use of low values. The application of this cutting speed range, together with the analysis of the feed influence, is one of the main novelties of this work.

**Table 2.** Cutting conditions.

$v_c$ (m/min)	$f$ (mm/r)	$a_p$ (mm)
40	0.05	1
60	0.10	
80	0.15	
	0.20	

Hence, 12 samples were machined (one for each cutting parameter combination). The used cutting tools were uncoated WC-Co inserts, with ISO reference DCMT 11T308-14 IC, a tool-tip angle of  $55^\circ$ , and a tip radius of 0.8 mm.

In order to analyze the surface roughness influence on microhardness (before and after a corrosion process), the roughness profile was obtained. It is necessary to point out that the evolution of the microgeometrical deviations as a function of the cutting parameters, in the dry machining of this alloy, was widely studied. Nevertheless, in this work, the microgeometrical deviations were measured with a double purpose. On one hand, they may be used as an element of control and comparison with previous research. On the other hand, they could be useful to analyze possible synergistic actions between cutting parameters, hardness, surface roughness, and corrosion behavior. For this purpose, a Mitutoyo portable roughness tester, model Mitutoyo SURFTTEST SJ-210, was used. The average roughness ( $Ra$ ) and the maximum height of the profile ( $Rz$ ) were used as parameters to evaluate the surface quality (Equations (1) and (2)).

$$Ra = \frac{1}{lr} \int_0^{lr} |Z(x)| dx, \quad (1)$$

$$Rz = Zp + Zv, \quad (2)$$

where  $lr$  is the sampling length,  $Z(x)$  is the profile height,  $Zp$  is the peak height, and  $Zv$  is the peak valley of the roughness profile.

Two measures were obtained along two different areas. The measurement was repeated along four specimen generatrix (G1–G4,  $90^\circ$  apart; Figure 2). Therefore, eight roughness profiles were obtained for each specimen. The surface roughness measurement was carried out according to the UNE-EN ISO 4288: 1998 standard [42]. The used parameters are indicated below.

- Filter: normal Gaussian distribution;
- Measurement or scan length ( $ls$ ):  $2.5 \mu\text{m}$ ;
- Basic or contact length ( $lc$ ): 0.8 mm.

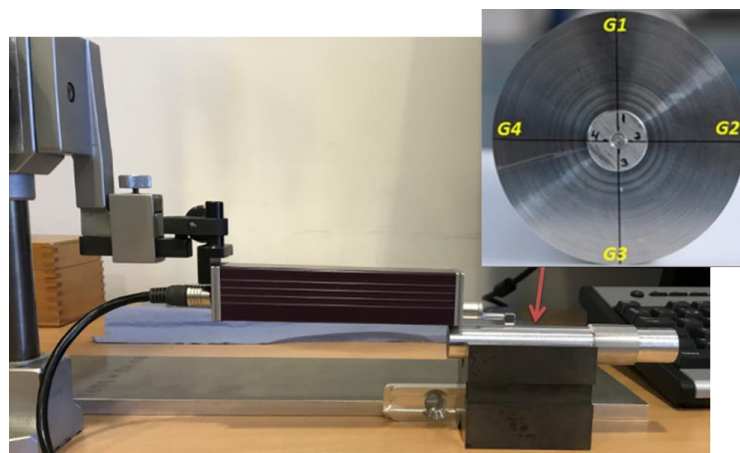


**Figure 2.** Roughness profile measurement set-up.

A Vickers hardness test was performed on each specimen, according to the UNE-EN ISO 6507-1: 2018 standard [43]. A non-machined specimen (stock bar) was used as a control element, to compare the results with the machined samples. The applied load was 0.05 kgf (0.05 HV), corresponding to a value of 0.49 N. The tests were carried out on two different generatrices, obtaining hardness results at four points (T1, T2, T3, and T4) on the same generatrix (Figure 1b). The hardness tests were carried out by using a MATSUZAWA MXT70 micro-hardness tester, with a pyramid-shaped indenter (with a

square diamond base and an angle between opposite faces of  $136^\circ$ ; Figure 3). The temperature of the measurement area was controlled, remaining within the standard limits of  $23 \pm 5^\circ\text{C}$  [43].

Once the surface hardness was measured, the corrosion process for the machined and non-machined samples was carried out. The samples were placed by immersion within a corrosive environment. For this purpose, a solution of deionized water and NaCl (3.5% concentration) was used, keeping the specimens in that environment for 72 h.

During the corrosion process, the corrosive medium temperature was continuously checked, remaining at  $26 \pm 1^\circ\text{C}$ . In addition, a pump was placed in the solution to keep the saline medium moving and to avoid NaCl stratification, ensuring the corrosion process homogeneity on the surface of all samples. After the corrosion process, the surface roughness profile was measured in every sample (following the same methodology). After that, the hardness tests were carried out once again, under the same conditions previously described.

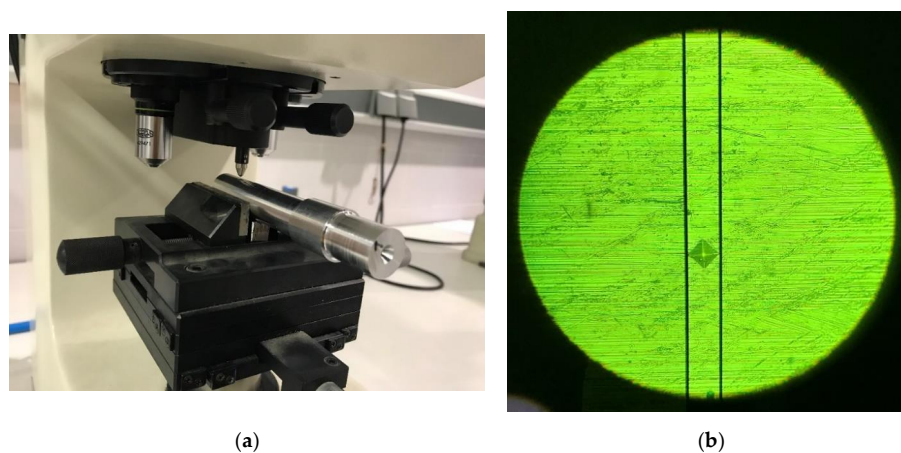


**Figure 3.** (a) Hardness test set-up; (b) generated mark in the test point.

Finally, scanning electron microscopy (SEM) and energy-dispersive spectroscopy (EDS) techniques were used in order to analyze the alloy microstructure and micro-composition, before and after machining. An etchant (2.5%  $\text{HNO}_3$ , 1.5%  $\text{HCl}$ , 1%  $\text{HF}$ ; 95%  $\text{H}_2\text{O}$ ) was used to show the grain structure. An image processing software was used to measure the grain size, according to the standard ASTM E112 “Standard Test Methods for Determining Average Grain Size” (Equations (3)–(5)).

$$N = 2^n A^{-1}, \quad (3)$$

$$n = n_A + Q, \quad (4)$$

$$Q = 2 \log_2 \left( \frac{\mu}{100} \right), \quad (5)$$

where  $N$  is the number of grains,  $n$  is the grain size,  $n_A$  is the apparent grain size,  $Q$  is the correction factor, and  $\mu$  is the micrograph magnification.

### 3. Results and Discussion

Figures 4 and 5 plot the evolution of  $R_a$  and  $R_z$ , respectively, as a function of the cutting parameters,  $v_c$  and  $f$ , before (Figures 3a and 4a) and after (Figures 3b and 4b) the corrosion process. These values were calculated as the average values of the experimental results, measured in four different lines along the specimens. Additionally, the  $R_a$  and  $R_z$  values of the non-machined sample were identified in the figures, in order to analyze the induced alterations by the machining process.

The results revealed that the feed was the most influential variable on surface roughness. Both parameters,  $R_a$  and  $R_z$ , showed a general trend to increase with  $f$ , regardless of  $v_c$ . This trend was more noticeable from  $f = 0.10$  to  $0.20$  mm/r. For samples before corrosion,  $R_a$  was three times higher for

$f = 0.10$  mm/r than for 0.20 mm/r. For samples after corrosion, the effect of  $f$  was amplified, reaching four-fold higher values for 0.20 mm/r than for 0.1 mm/r. The feed influence was less evident in the range of low  $f$  applied (0.05–0.10 mm/r). For these low  $f$  values,  $Ra$  and  $Rz$  showed similar values to samples before machining.

With regard to  $v_c$ , no significant modifications were observed in  $Ra$  or  $Rz$  when this parameter was modified. Therefore, the effect of the natural roughness, induced by the feed, was predominant over the thermal effects that cutting speed variations may have caused during the cutting process, such as the appearance of built-up edge (BUE), which may have affected the surface quality [5,44]. In the dry machining of this alloy, this indirect adhesion tool wear is usually a consequence of the thermo-mechanical effects at high feed. Nevertheless, the effect of cutting speed becomes more relevant for low feed, giving rise to BUE with higher intensity for higher cutting speed values. However, the low cutting speed applied in this research made this effect less noticeable and, as a result, the cutting speed effect on surface roughness was almost negligible [45–47].

It is necessary to point out that all these observations are in good agreement with previous research, in connection with the parametric analysis of surface roughness in the dry turning of the 2000 and 7000 aluminum alloys series [45,47,48].

Regarding the corrosion process, no significant changes in  $Ra$  were observed. However, the dispersion in the results seemed to be a little bit higher. This fact was more evident for  $Rz$ . These results may be explained considering that  $Ra$  was calculated as an average value of peaks and valleys of the roughness profile, while  $Rz$  was obtained as the maximum height of the profile. The appearance of pitting and intergranular corrosion, mainly in the inter-metallic elements ( $Al_{23}CuFe_4$ ), resulted in surface irregularities that may have affected the values of the microgeometrical deviations at one point (Figure 6). This effect was softened in the calculation of average values to obtain  $Ra$ .

In addition, an increment in  $Rz$  was observed after the corrosion process, regardless of  $v_c$  and  $f$ . Only for the highest  $f$  (0.20 mm/r) was this increment slightly higher. A poorer surface quality, at high  $f$ , resulted in a higher corrosion effect, and vice versa. Hence,  $f$  seemed to be a little more influent only in the highest range of the tested values.

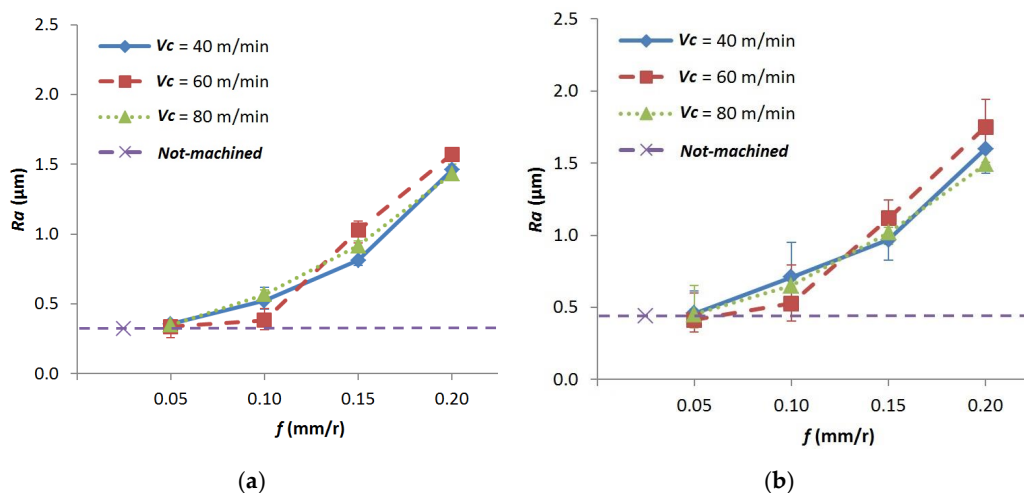


**Figure 4.** Average roughness ( $Ra$ ) as a function of feed ( $f$ ) and cutting speed ( $v_c$ ), (a) before and (b) after a corrosion process.

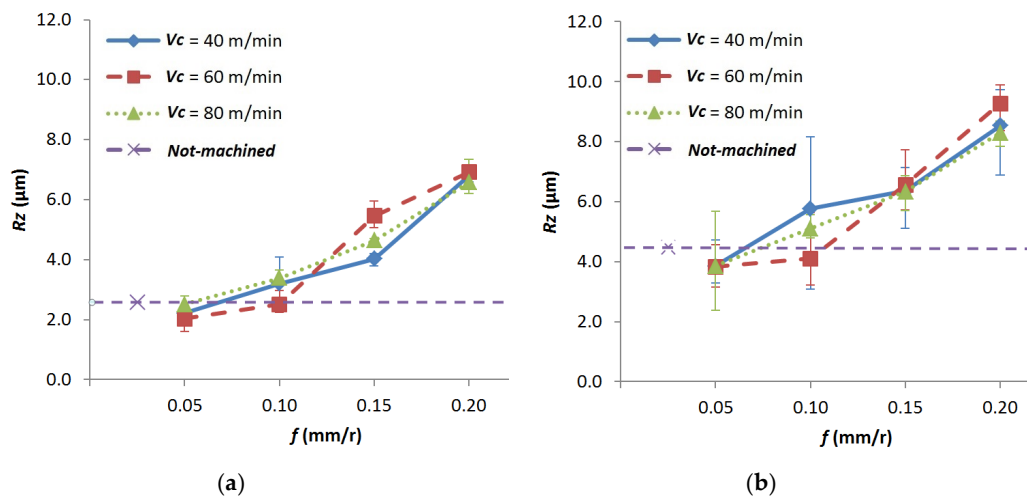


**Figure 5.** Maximum height of the profile ( $R_z$ ) as a function of feed ( $f$ ) and cutting speed ( $v_c$ ), (a) before and (b) after a corrosion process.

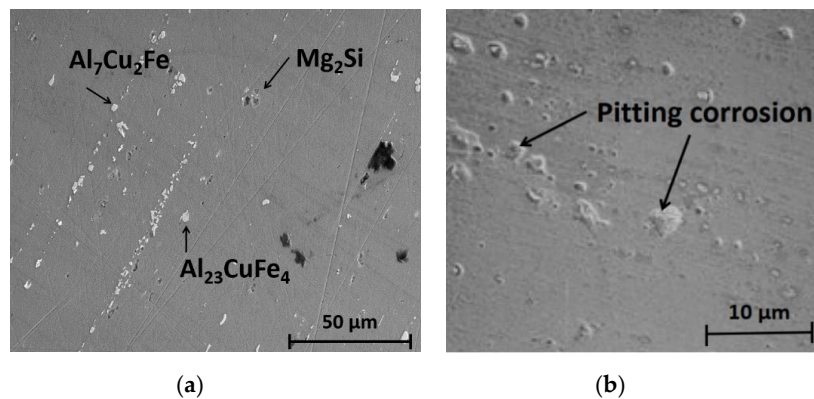


**Figure 6.** (a) SEM image of the microstructural composition of the UNS A97075 alloy tested (before machining and corrosion processes); (b) SEM image of the pitting corrosion effect on the machined surface.

Figure 7 shows the average microhardness values as a function of  $v_c$  and  $f$ , after and before the corrosion process, for the machined samples. In addition, the microhardness values for the non-machined samples are also plotted, as reference values.

In general, a surface microhardness ( $HV$ ) increment was observed in all samples, after machining and before corrosion (Figure 7a), regardless of  $v_c$  and  $f$ . Its value was increased by 25% for a certain cutting parameter combination ( $f = 0.15$  mm/r;  $v_c = 60$  m/min), regarding the non-machined sample. This fact can be explained taking into account that machining resulted in very aggressive conditions (high pressures and temperatures) in the cutting area, both in the tool and the part. The compression forces gave rise to a plastic deformation of the machined surface [49], as well as microstructural alterations (finer grain structure), which resulted in strain hardening [29] (Figure 8).

Regarding the cutting speed influence on microhardness, Figure 7a shows very similar  $HV$  mean values for  $v_c = 40$  and 80 m/min, whereas its mean value seemed to increase for  $v_c = 60$  m/min, for the intermediate range of  $f$  (0.10 and 0.15 mm/r). In addition, higher dispersion in the experimental results was observed for this cutting parameter combination. With regard to  $f$ , the best results (the highest  $HV$ ) were obtained for  $f = 0.10$  and 0.15 mm/r. When these values were combined with the intermediate  $v_c$  tested value (60 m/min),  $HV$  reached a difference of 25% compared to other cutting speed values (40 and 80 m/min). For other  $f$  (0.05 and 0.20 mm/r) and  $v_c$  (40 and 80 m/min), a clear  $HV$  trend as a function of the cutting parameters was not observed.

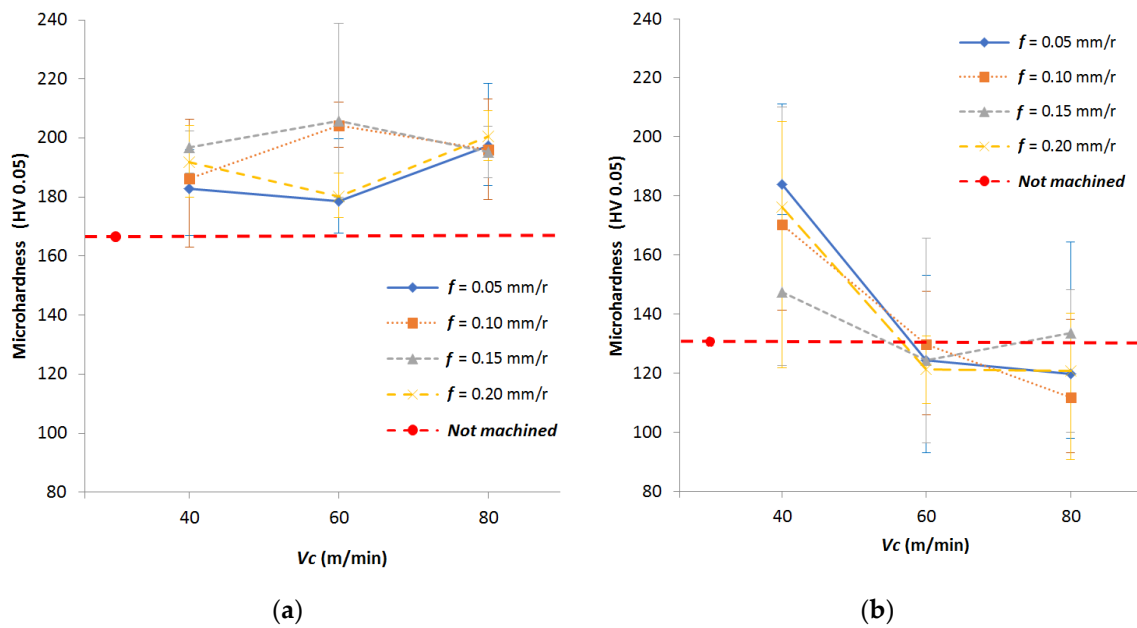


Figure 7. Surface microhardness (a) before corrosion and (b) after corrosion.

Therefore, the highest  $HV$  results were obtained when the intermediate range of cutting speed and feed values was applied. These results may be explained considering the effect that  $f$  and  $v_c$  produce on the surface microstructure. On one hand,  $f$  increments usually produce a higher plastic deformation on the machined surface due to mechanical effects (strain hardening), whereas the thermal effects are usually lower [49]. Therefore, a finer grain microstructure is obtained, giving rise to  $HV$  increments. On the other hand,  $v_c$  increments result in higher temperature in the cutting area [28]. The produced heat is removed from the cutting area by the chip, the tool, and the part. At high cutting speeds, most of the energy is dissipated through the chip. For low cutting speeds (such as those used in this work), the dissipated energy by the chip becomes lower; thus, the dissipated heat through the tool and the part is increased. This fact results in a grain size increment and an  $HV$  reduction [29]. When  $v_c$  is increased (within this low range), this effect becomes more relevant.

Hence, for low  $f$  (0.05 mm/r) and  $v_c$  (40 m/min), mechanical effects predominated over thermal effects. The grain microstructure was finer than in the non-machined part (from 18.35 to 15.36  $\mu\text{m}$  average grain size), and  $HV$  was higher (Figure 8c). For the intermediate range of  $f$  (0.10–0.15 mm/r) and  $v_c$  (60 m/min), the mechanical effects were stronger (Figure 8b). Thermal effects were increased but were not high enough to compensate for the mechanical effects. As a result, the grain microstructure was finer (14.04  $\mu\text{m}$  average grain size) than for low  $f$  and  $v_c$ , and  $HV$  was increased.

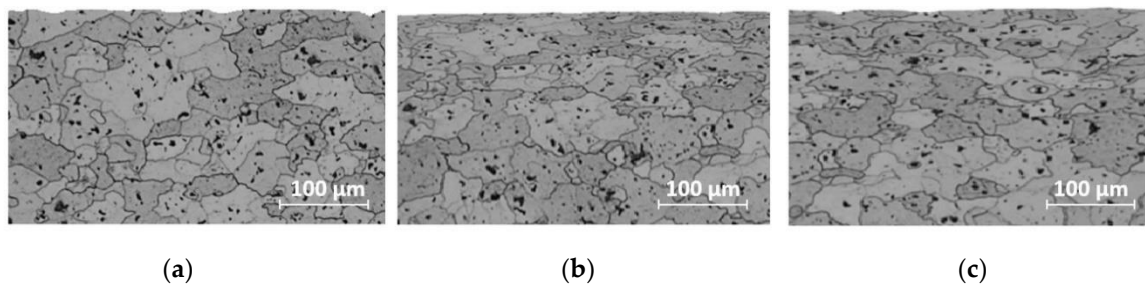


Figure 8. SEM images of the surface microstructure: (a) non-machined; (b)  $v_c = 60$  m/min and  $f = 0.15$  mm/r; (c)  $v_c = 40$  m/min and  $f = 0.05$  mm/r.

Finally, for the highest  $v_c$  (80 m/min), the thermal effects became more relevant and compensated for the mechanical effects. Therefore, the grain size was greater and  $HV$  was reduced, reaching a

similar size to that for low  $f$  values. Consequently, mechanical and thermal effects were mixed, and the feed mechanical effects could not be neglected against the thermal effects of cutting speed, within the range of the tested  $v_c$  values. This fact made it more difficult to obtain a clear trend of  $HV$  as a function of the cutting parameters.

With regard to the  $HV$  results after corrosion, a general microhardness reduction was observed in the samples, both before and after machining (Figure 7b). In addition, a higher dispersion was obtained in all the range of the tested cutting parameters. The irregularities in the surface, due to pitting corrosion, resulted in a higher dependence on the surface point where  $HV$  was measured. Similar average values were obtained for  $v_c = 60$  and  $80$  m/min and the sample before machining. The average value seemed to be higher only for  $v_c = 40$  m/min. However, it was difficult to establish a general trend, given the high level of dispersion that the results showed. Therefore, the corrosion process negatively affected microhardness, but it was not possible to establish a direct relationship between cutting parameters, surface roughness, and microhardness after a corrosion process.

#### 4. Conclusions

In this work, the cutting speed and feed influence on the microhardness of dry-turned UNS A97075-T6 alloy samples was analyzed. The results were compared with the non-machined samples, before and after a corrosion process, in order to study the possible connection between cutting parameters, microgeometrical deviations, microhardness, and corrosion.

The microgeometrical deviations, evaluated through  $Ra$  and  $Rz$ , showed a general trend to increase with feed. However, no significant modifications were observed as a function of cutting speed. The natural roughness, induced by the feed, was predominant over the cutting speed thermal effects (such as surface alterations originated by the indirect adhesion tool wear). These observations are in good agreement with previous research regarding parametric analysis on surface roughness for the 7000 aluminum alloys series.

In addition, no significant changes in  $Ra$  were observed after corrosion. However, an  $Rz$  increment was observed, regardless of feed and cutting speed. For the highest feed value ( $0.20$  mm/r), this increment was slightly higher. Therefore, feed seemed to be more influential for the highest tested values. Additionally, the dispersion in the results seemed to be higher for  $Ra$ . This fact was more evident for  $Rz$ . The appearance of surface alterations, due to pitting corrosion, resulted in a higher dispersion of the maximum height of the surface profile ( $Rz$ ). This effect was softer for  $Ra$ , because it was calculated as an average value of the surface profile deviations.

In general, a surface microhardness ( $HV$ ) increment was observed in all samples, after machining and before corrosion, regardless of  $v_c$  and  $f$ . The highest microhardness was obtained for the intermediate cutting speed ( $60$  m/min) and feed ( $0.10$ – $0.15$  mm/r) values. For low feed and cutting speed, mechanical effects predominated over thermal effects. This fact resulted in finer microstructure than in the non-machined part, giving rise to microhardness increments. For the intermediate range of feed and cutting speed, the mechanical effects were stronger. The thermal effects were increased, but not high enough to compensate for the mechanical effects. As a result, the grain microstructure was finer than for low feed and cutting speed. Finally, for the highest cutting speed ( $80$  m/min), the thermal effects were more relevant and compensated for the mechanical effects, increasing the grain size and reducing the microhardness. Therefore, the mechanical effects, produced by feed, should not be neglected against the thermal effects, produced by cutting speed, within the low range of tested cutting speed.

A general microhardness reduction was observed in the samples after corrosion. However, a higher dispersion in the results was obtained in a wide range of cutting parameters analyzed, due to the irregularities in the surface produced by pitting corrosion. Therefore, the corrosion process negatively affected microhardness, but it was not possible to establish a direct relationship between cutting parameters, surface roughness, and microhardness after a corrosion process.

It is necessary to highlight that previous works in this regard usually focused on high-speed values of cutting speed, typically used on non-hybridized alloy. Under these conditions, the cutting speed is the most relevant cutting parameter and, therefore, thermal effects predominate over the mechanical ones. However, there is a gap in knowledge regarding the analysis of the possible influence of feed when low cutting speeds are used. Hence, this work covers this gap.

Finally, it is necessary to point out that this work is framed within a broader research line, currently in development, regarding the analysis of the cutting parameter influence on the surface integrity of UNS A97075 alloy, turned under dry conditions. This research line focuses on analyzing the relationship between cutting parameters, surface topography, and mechanical properties.

**Author Contributions:** S.M.-B. and F.J.T.V. conceptualized and designed the experiments; S.M.-B. performed the experiments; S.M.-B., F.J.T.V., C.B.G., and L.S.H. analyzed the data; S.M.-B., F.J.T.V., and C.B.G. wrote the paper; L.S.H. revised the paper. All authors have read and agreed to the published version of the manuscript.

**Funding:** This research received no external funding.

**Acknowledgments:** The authors thank the University of Malaga-Andalucia Tech Campus of International Excellence for its economic contribution to this paper.

**Conflicts of Interest:** The authors declare no conflicts of interest.

## References

- Morinaga, M. A Quantum Approach to Alloy Design. In *Aluminum Alloys and Magnesium Alloys*; Elsevier: Amsterdam, The Netherlands, 2019; pp. 95–130.
- Campbell, F.C. *Manufacturing Technology for Aerospace Structural Materials*; Elsevier Science: Oxford, UK, 2006.
- Bencherghi, D.; Svoboda, C. *Aircraft Design*; Aerospace: Washington, DC, USA, 2012; Volume 50, p. 28.
- Martín Béjar, S.; Trujillo Vilches, F.J.; Bermudo Gamboa, C.; Sevilla Hurtado, L. Parametric analysis of macro-geometrical deviations in dry turning of UNS A97075 (Al-Zn) alloy. *Metals* **2019**, *9*, 1141. [[CrossRef](#)]
- Suraratchai, M.; Limido, J.; Mabru, C.; Chieragatti, R. Modelling the influence of machined surface roughness on the fatigue life of aluminium alloy. *Int. J. Fatigue* **2008**, *30*, 2119–2126. [[CrossRef](#)]
- Hernández-González, L.W.; Pérez-Rodríguez, R.; Dumitrescu, L.; Montero-Sarmiento, R. Estudio de la influencia de los parámetros de corte en la integridad superficial y las desviaciones durante el fresado del acero AISI 1010. *Revista Tecnología en Marcha* **2015**, *28*, 26–41. [[CrossRef](#)]
- M'saoubi, R.; Outeiro, J.C.C.; Chandrasekaran, H.; Dillon, O.W.; Jawahir, I.S.S. A review of surface integrity in machining and its impact on functional performance and life of machined products. *Int. J. Sustain. Manuf.* **2008**, *1*, 203. [[CrossRef](#)]
- Matsumoto, Y.; Hashimoto, F.; Lahoti, G. Surface integrity generated by precision hard turning. *CIRP Ann.-Manuf. Technol.* **1999**, *48*, 59–62. [[CrossRef](#)]
- Abrão, A.M.; Ribeiro, J.L.S.; Davim, J.P. Surface Integrity. In *Machining of Hard Materials*; Springer Science & Business Media: New York, NY, USA, 2011; pp. 115–141.
- Goncharenko, A.V. Aeronautical and Aerospace Material and Structural Damages to Failures: Theoretical Concepts. *Int. J. Aerosp. Eng.* **2018**, *2018*, 4126085. [[CrossRef](#)]
- Benedicto, E.; Carou, D.; Rubio, E.M. Technical, Economic and Environmental Review of the Lubrication/Cooling Systems Used in Machining Processes. *Procedia Eng.* **2017**, *184*, 99–116. [[CrossRef](#)]
- Kopac, J.; Pusavec, F.; Krolczyk, G. Cryogenic machining, surface integrity and machining performance. *Arch. Mater. Sci. Eng.* **2015**, *71*, 83–93.
- Krolczyk, G.M.; Maruda, R.W.; Krolczyk, J.B.; Wojciechowski, S.; Mia, M.; Nieslony, P.; Budzik, G. Ecological trends in machining as a key factor in sustainable production—A review. *J. Clean. Prod.* **2019**, *218*, 601–615. [[CrossRef](#)]
- Saleem, W.; Zain-ul-abdein, M.; Ijaz, H.; Salmeen Bin Mahfouz, A.; Ahmed, A.; Asad, M.; Mabrouki, T. Computational Analysis and Artificial Neural Network Optimization of Dry Turning Parameters—AA2024-T351. *Appl. Sci.* **2017**, *7*, 642. [[CrossRef](#)]
- Do, T.-V.; Hsu, Q.-C. Optimization of Minimum Quantity Lubricant Conditions and Cutting Parameters in Hard Milling of AISI H13 Steel. *Appl. Sci.* **2016**, *6*, 83. [[CrossRef](#)]

16. Vilches, F.; Hurtado, L.; Fernández, F.; Gamboa, C. Analysis of the Chip Geometry in Dry Machining of Aeronautical Aluminum Alloys. *Appl. Sci.* **2017**, *7*, 132. [[CrossRef](#)]
17. Kavitha, K.; Vijayan, R.; Sathishkumar, T. Fibre-metal laminates: A review of reinforcement and formability characteristics. *Mater. Today Proc.* **2019**. [[CrossRef](#)]
18. Lu, J.; Song, Y.; Hua, L.; Zheng, K.; Dai, D. Thermal deformation behavior and processing maps of 7075 aluminum alloy sheet based on isothermal uniaxial tensile tests. *J. Alloys Compd.* **2018**, *767*, 856–869. [[CrossRef](#)]
19. Syed, A.K.; Zhang, X.; Moffatt, J.E.; Fitzpatrick, M.E. Effect of temperature and thermal cycling on fatigue crack growth in aluminium reinforced with GLARE bonded crack retarders. *Int. J. Fatigue* **2017**, *98*, 53–61. [[CrossRef](#)]
20. Caruso, S.; Rotella, G.; Del Prete, A.; Umbrello, D. Finite Element Modeling of Microstructural Changes in Hard Machining of SAE 8620. *Appl. Sci.* **2019**, *10*, 121. [[CrossRef](#)]
21. Meng, X.; Lin, Z.; Wang, F. Investigation on corrosion fatigue crack growth rate in 7075 aluminum alloy. *Mater. Des.* **2013**, *51*, 683–687. [[CrossRef](#)]
22. Yang, X.W.; Li, W.Y.; Li, H.Y.; Yao, S.T.; Sun, Y.X.; Mei, L. Microstructures and microhardness for sheets and TIG welded joints of TA15 alloy using friction stir spot processing. *Trans. Nonferrous Met. Soc. China* **2018**, *28*, 55–65. [[CrossRef](#)]
23. Privezentsev, D.; Zhiznyakov, A.; Kulkov, Y. Analysis of the Microhardness of Metals Using Digital Metallographic Images. *Mater. Today Proc.* **2019**, *11*, 325–329. [[CrossRef](#)]
24. Jirapattarasilp, K.; Kuptanawin, C. Effect of Turning Parameters on Roundness and Hardness of Stainless Steel: SUS 303. *Procedia-Soc. Behav. Sci.* **2012**, *3*, 160–165. [[CrossRef](#)]
25. Sasahara, H. The effect on fatigue life of residual stress and surface hardness resulting from different cutting conditions of 0.45%C steel. *Int. J. Mach. Tool Manuf.* **2004**, *45*, 131–136. [[CrossRef](#)]
26. Akkurt, A. The effect of cutting process on surface microstructure and hardness of pure and Al 6061 aluminium alloy. *Eng. Sci. Technol. Int. J.* **2015**, *18*, 303–308. [[CrossRef](#)]
27. Kurkute, V.; Chavan, S.T. Modeling and Optimization of surface roughness and microhardness for roller burnishing process using response surface methodology for Aluminum 63400 alloy. *Procedia Manuf.* **2018**, *20*, 542–547. [[CrossRef](#)]
28. Surya Sundara Rao, K.; Viswanath Allamraju, K. Effect on Micro-Hardness and Residual Stress in CNC Turning of Aluminium 7075 Alloy. *Mater. Today Proc.* **2017**, *4*, 975–981. [[CrossRef](#)]
29. Rotella, G.; Dillon, O.W.; Umbrello, D.; Settineri, L.; Jawahir, I.S. Finite element modeling of microstructural changes in turning of AA7075-T651 Alloy. *J. Manuf. Process.* **2013**, *15*, 87–95. [[CrossRef](#)]
30. Campbell, C.E.; Bendersky, L.A.; Boettinger, W.J.; Ivester, R. Microstructural characterization of Al-7075-T651 chips and work pieces produced by high-speed machining. *Mater. Sci. Eng. A* **2006**, *430*, 15–26. [[CrossRef](#)]
31. Sravanthi, M.; Manjunatha, K.G. Corrosion Studies of As Casted and Heat Treated Aluminium-7075 Composites. *Mater. Today Proc.* **2018**, *5*, 22581–22594. [[CrossRef](#)]
32. Dong, H. *Surface Engineering of Light Alloys: Aluminium, Magnesium and Titanium Alloys*; CRC Press: Amsterdam, The Netherlands, 2010.
33. Guérin, M.; Alexis, J.; Andrieu, E.; Blanc, C.; Odemer, G. Corrosion-fatigue lifetime of Aluminium-Copper-Lithium alloy 2050 in chloride solution. *Mater. Des.* **2015**, *87*, 681–692. [[CrossRef](#)]
34. Liu, B.; Zhang, X.; Zhou, X.; Hashimoto, T.; Wang, J. The corrosion behaviour of machined AA7150-T651 aluminium alloy. *Corros. Sci.* **2017**, *126*, 265–271. [[CrossRef](#)]
35. Dong, P.; Sun, D.; Wang, B.; Zhang, Y.; Li, H. Microstructure, microhardness and corrosion susceptibility of friction stir welded AlMgSiCu alloy. *Mater. Des.* **2014**, *54*, 760–765. [[CrossRef](#)]
36. Wang, X.; Nie, M.; Wang, C.T.; Wang, S.C.; Gao, N. Microhardness and corrosion properties of hypoeutectic Al-7Si alloy processed by high-pressure torsion. *Mater. Des.* **2015**, *83*, 193–202. [[CrossRef](#)]
37. Donatus, U.; Viveiros, B.V.G.; de Alencar, M.C.; de Ferreira, R.O.; Milagre, M.X.; Costa, I. Correlation between corrosion resistance, anodic hydrogen evolution and microhardness in friction stir weldment of AA2198 alloy. *Mater. Charact.* **2018**, *144*, 99–112. [[CrossRef](#)]
38. Sherafat, Z.; Paydar, M.H.; Ebrahimi, R. Fabrication of Al7075/Al, two phase material, by recycling Al7075 alloy chips using powder metallurgy route. *J. Alloys Compd.* **2009**, *487*, 395–399. [[CrossRef](#)]
39. Zhenchao, Y.; Yang, X.; Yan, L.; Jin, X.; Quandai, W. The effect of milling parameters on surface integrity in high-speed milling of ultrahigh strength steel. *Ann. DAAAM Proc.* **2019**, *30*, 753–757. [[CrossRef](#)]

40. Yue, T.M.; Yu, J.K.; Man, H.C. Corrosion behavior of aluminum 2009/SiC composite. *Mater. Today Proc.* **2009**, *2*, 1069–1072.
41. Bienvenido, R.; Díaz Vázquez, J.E.; Botana, J.; Cano, M.J.; Marcos, M. Preliminary study of the influence of machining conditions in the response to corrosion of UNS-A92024 alloy. *Proc. Adv. Mater Res.* **2010**, *107*, 117–121. [[CrossRef](#)]
42. International Standarding Organization. *ISO 1302:2002. Geometrical Product Specifications (GPS)—Indication of Surface Texture in Technical Product Documentation*; International Standarding Organization: Geneva, Switzerland, 2002.
43. International Standarding Organization. *ISO 6507-1:2018. Metallic Materials—Vickers Hardness Test-Part 1: Test Method*; International Standarding Organization: Geneva, Switzerland, 2018.
44. Tank, K.; Shetty, N.; Panchal, G.; Tukrel, A. Optimization of turning parameters for the finest surface roughness characteristics using desirability function analysis coupled with fuzzy methodology and ANOVA. *Mater. Today Proc.* **2018**, *5*, 13015–13024. [[CrossRef](#)]
45. Trujillo, F.J.; Marcos Bárcena, M.; Sevilla, L. Experimental Prediction Model for Roughness in the Turning of UNS A97075 Alloys. *Mater. Sci. Forum* **2014**, *797*, 59–64. [[CrossRef](#)]
46. Torres, A.; Puertas, I.; Luis, C.J. Surface roughness analysis on the dry turning of an Al-Cu alloy. *Procedia Eng.* **2015**, *132*, 537–544. [[CrossRef](#)]
47. Rubio, E.M.; Camacho, A.M.; Sánchez-Sola, J.M.; Marcos, M. Surface roughness of AA7050 alloy turned bars: Analysis of the influence of the length of machining. *Proc. J. Mater. Proces. Technol.* **2005**, *162–163*, 682–689. [[CrossRef](#)]
48. Bandeira, R.M.; van Drunen, J.; Garcia, A.C.; Tremiliosi-Filho, G. Influence of the thickness and roughness of polyaniline coatings on corrosion protection of AA7075 aluminum alloy. *Electrochim. Acta* **2017**, *240*, 215–224. [[CrossRef](#)]
49. Ajithkumar, J.; Xavier, M.A. Cutting Force and Surface Roughness Analysis During Turning of Al 7075 Based Hybrid Composites. *Procedia Manuf.* **2019**, *30*, 180–187. [[CrossRef](#)]



© 2020 by the authors. Licensee MDPI, Basel, Switzerland. This article is an open access article distributed under the terms and conditions of the Creative Commons Attribution (CC BY) license (<http://creativecommons.org/licenses/by/4.0/>).